Validity of the Parabolic Effective Mass Approximation in Silicon and Germanium n-MOSFETs With Different Crystal Orientations

Jan-Laurens P. J. van der Steen, *Student Member, IEEE*, David Esseni, *Senior Member, IEEE*, Pierpaolo Palestri, *Member, IEEE*, Luca Selmi, *Member, IEEE*, and Raymond J. E. Hueting, *Senior Member, IEEE*

***Abstract*—This paper investigates the validity of the parabolic effective mass approximation (EMA), which is almost universally used to describe the size and bias-induced quantization in n-MOSFETs. In particular, we compare the EMA results with a full-band quantization approach based on the linear combination of bulk bands (LCBB) and study the most relevant quantities for the modeling of the mobility and of the on-current of the devices, namely, the minima of the 2-D subbands, the transport masses, and the electron density of states. Our study deals with both silicon and germanium n-MOSFETs with different crystal orientations and shows that, in most cases, the validity of the EMA is quite satisfactory. The LCBB approach is then used to calculate the values of the effective masses that help improve the EMA accuracy. There are crystal orientations, however, where the 2-D energy dispersion obtained by the LCBB method exhibits features that are difficult to reproduce with the EMA model.**

***Index Terms*—Band structure, effective mass approximation, full-band, quantization models, quantum confinement.**

I. Introduction

NANOSTRUCTURED devices are being extensively investigated for their possible application in CMOS and post-CMOS technologies. The most interesting examples include the fully depleted, ultrathin film silicon-on-insulator (UT-SOI) MOSFETs [1]–[6] and the nanowire transistors, which are promising candidates for the ultimate CMOS downscaling [7]–[11]. The engineering options for the nano-MOSFETs include the choice of the semiconductor and its crystallographic orientation [12]–[15], as well as the biaxial or uniaxial mechanical strain [16]–[19]; all of them deserve an accurate and extensive evaluation by means of device simulations.

Most of the above design knobs impact the electrical characteristics of a metal–oxide–semiconductor (MOS) transistor through its band structure in the plane of the transport, which affects both the injection velocity at the virtual source, hence the maximum *ballistic on-current* $I_{\rm BL}$ of the device [20], [21], and the scattering rates, which still significantly limit the *real on-current* of the devices [22], [23]. Thus, for the simulation of UT-SOI transistors, we need a quantization model to calculate the band structure as a function of the 2-D wave vector $\mathbf{k}$ in the transport plane (i.e., the 2-D band structure), which should be both computationally efficient and accurate even for a very small semiconductor thickness $T_{\rm SCT}$. The computational efficiency is particularly critical for the development of a multi-subband Monte Carlo simulator [24], where the band structure must be computed at each section of the MOSFET and each time the electrostatic potential is updated.

The effective mass approximation (EMA) is almost universally used both in the semiclassical transport models [24]–[28] and in several recent studies that employ a quantum transport treatment [12], [13], [29]. In the semiclassical picture, the band structure at each section of the device is obtained by solving the 1-D quantization problem set by the confining potential energy in the direction normal to the semiconductor–oxide interface. In this case, when a parabolic energy dispersion is assumed in the quantization direction, the EMA results in a Schrödinger-like equation in the real space that provides the minima of the subbands. Then, an analytic energy dispersion in the transport plane (i.e., as a function of the 2-D wave vector $\mathbf{k}$) is added to the subband minimum [24], [26]–[28]. Thus, in such an EMA model, the quantization produces a shift in the subband minima; while, it does not affect the energy dispersion inside each subband.

However, for very small $T_{\rm SCT}$ values, the strong quantum mechanical confinement can yield significant deviations from the simple EMA results mainly in terms of: 1) different values for the minima of the 2-D subbands; and 2) distortion of the energy dispersion in the transport plane, with a resulting change in the transport masses and in the 2-D effective density of states (DOS). Such effects have been recently investigated for the silicon nanowire transistors by using the tight-binding approach [30].

In this paper, we extend the work presented in [31] and investigate the validity of the EMA quantization model for the silicon and the germanium n-MOSFETs with different crystal orientations by means of a systematic comparison to the band structure that is calculated with the linear combination of bulk bands (LCBB) [32]–[34]. More precisely, we start by

Manuscript received April 5, 2007. This work was supported in part by the Italian MIUR under (PRIN project 2004) and the EU under project SINANO NoE, IST-506844 and the PullNano integrated project. The review of this paper was arranged by Editor S. Datta.

J.-L. P. J. van der Steen and R. J. E. Hueting are with the MESA+ Institute for Nanotechnology, University of Twente, 7500 Enschede, The Netherlands (e-mail: j.l.p.j.vandersteen@utwente.nl).

D. Esseni, P. Palestri, and L. Selmi are with the Department of Electrical, Mechanical and Management Engineering (DIEGM), University of Udine, 33100 Udine, Italy (e-mail: esseni@uniud.it).

Digital Object Identifier 10.1109/TED.2007.900417

discussing the differences in the minima of the 2-D subbands that are obtained with either the EMA or the LCBB model. Then, we extract the transport masses from the LCBB band structure for different $T_{\rm SCT}$ values and compare the numerically calculated 2-D DOS of the LCBB method with the analytical expressions of the EMA model. The overall results on the validity of the EMA approach are quite reassuring, and the accuracy of the EMA model can be improved by adjusting the transport masses for very thin semiconductor thicknesses.

II. LCBB Band Structure Calculation

The LCBB approach is an accurate full-band method for the calculation of the band structure in nanostructured devices, and it is based on the expansion of the *unknown* eigenfunction in terms of the bulk Bloch functions of the constituent semiconductor. As implied by (1), shown at the bottom of the page, we used a confining potential energy to mimic the band discontinuity at the semiconductor–oxide interface; specifically, we embraced a single material approximation, which seems reasonable for the semiconductor–oxide heterojunctions where the band discontinuity is very large.

If we let z be the quantization direction and $U(z)$ the confining potential energy, then, for each $\mathbf{k}$ vector in the transport plane, the allowed energies $\epsilon_\mu(\mathbf{k})$ are calculated by solving the eigenvalue problem [34] where μ is the index of the eigenvalue (i.e., the subband index), $A_\mu^{(n)}(\mathbf{k}, k_z)$ denotes the coefficients of the *unknown* eigenfunction, $U_T(q_z)$ is the Fourier transform of $U(z)$, $(2\pi/L)$ is the spacing used for the discretization of k_z, and G_z is the magnitude of a reciprocal lattice vector in the k_z direction. Furthermore, $E_{\rm FB}^{(n)}(\mathbf{k}, k_z)$ is the energy in the nth band of the bulk crystal conduction band, and $f_{k_z,k_z'}^{(n,n')}(\mathbf{k}, G_z)$ denotes an appropriate *overlap integral* of the periodic parts $u_{n,\mathbf{k},k_z}$ of the Bloch functions [34], [35]. The index n' runs over the number $n_{\rm FB}$ of bands of the bulk crystal included in the calculations; in all the calculations, we have used the two lowest bands of the bulk crystal conduction band.

From (1) we clearly see that, in the LCBB method we have to calculate the Fourier transform of the potential $U(z)$ so that $U(z)$ has to feature a finite potential energy barrier at the semiconductor–oxide interface, which is hereafter denoted with U_B. Furthermore, (1) also clarifies that the full-band energy $E_{\rm FB}^{(n)}(\mathbf{k}, k_z)$ of the constituent semiconductor is an input of the LCBB method. We have used the well-established nonlocal-pseudopotential (NLP, [36]) method to determine both the full-band dispersion $E_{\rm FB}^{(n)}(\mathbf{k}, k_z)$ and the overlap factors $f_{k_z,k_z'}^{(n,n')}(\mathbf{k}, G_z)$ that enter (1). The parameters for the NLP procedure were taken from [36] for silicon and from [37] for germanium.

TABLE I
Parameters of the EMA Model for Different Materials and Quantization Directions. For Each Valley, n_ν Is the Degeneracy, m_z Is the Quantization Mass, and m_{le} and m_{te} Are the Longitudinal and Transverse Mass of the Elliptic Energy Dispersion Around the Minimum (in Unit of m_0), Respectively. ΔE Denotes the Energy Split Between the Valleys in the Bulk Semiconductor. The Effective Masses m_z, m_{le}, and m_{te} Have Been Obtained as Explained in [40] From the Longitudinal and the Transverse Masses of the Bulk Crystal Energy Dispersion by Using the Values $0.916m_0$ and $0.19m_0$ for the Δ Valleys of the Bulk Silicon, $1.6m_0$ and $0.093m_0$ for the Λ Valleys, $0.888m_0$ and $0.194m_0$ for the Δ Valleys, and $0.05m_0$ for the Γ Valley of the Bulk Germanium

	Quant.Dir.	Valley	n_ν	ΔE [eV]	m_{te}	m_{le}	m_z
Si	(001)	$D_{0.916}$	2	0	0.190	0.190	0.916
		$D_{0.19}$	4	0	0.190	0.916	0.190
	(110)	$D_{0.315}$	4	0	0.190	0.553	0.315
		$D_{0.19}$	2	0	0.190	0.916	0.190
	(111)	$D_{0.268}$	6	0	0.190	0.674	0.268
Ge	(110)	$L_{0.25}$	2	0	0.093	0.595	0.25
		$L_{0.093}$	2	0	0.093	1.60	0.093
		$D_{0.318}$	4	0.189	0.194	0.541	0.318
		$D_{0.194}$	2	0.189	0.194	0.888	0.194
		$\Gamma_{0.05}$	1	0.145	0.05	0.05	0.05

All the results shown in the following of the paper have been obtained by solving directly (1) with no further approximations. As explained in [34], the k_z values included in (1) must vary in a periodicity interval of the reciprocal lattice space along the k_z direction, namely, in an interval of length 2, $2\sqrt{2}$, and $\sqrt{3}$ for the (100), (110), and (111) quantization direction, respectively. Throughout the paper, we express the wave vectors in units of $(2\pi/a_0)$, where the lattice constant a_0 is 0.543 and 0.565 nm for silicon and germanium, respectively. The 2-D band structure is calculated with the LCBB method by varying the wave vector $\mathbf{k}$ in (1), where $\mathbf{k}$ plays the role of a parameter.

Fig. 1 illustrates the lowest subband versus the 2-D $\mathbf{k}$ vector for the inversion layer of a Si(100) SOI MOSFET. The $D_{0.916}$ 2-D valley is clearly observed at the point $\mathbf{k} = (0, 0)$, whereas the $D_{0.19}$ valleys are at the points $\mathbf{k} = (\pm 0.85, 0)$ and $\mathbf{k} = (0, \pm 0.85)$ (see Table I for the labels of the valleys). As it can be seen in Fig. 1, in general, the valleys of the 2-D electron gas are not located at the point $\mathbf{k} = (0, 0)$; hence, when we analyze the energy dispersion of a 2-D valley with the LCBB method, we must solve (1) along the lines in the $\mathbf{k}$ plane that run across the minimum of the valley. Furthermore, the value of $\mathbf{k}$ in the plots that correspond to a given valley is always obtained as the displacement with respect to the $\mathbf{k}$ point that corresponds to the minimum of the valley [i.e., $\mathbf{k} = (0, 0)$ for the $D_{0.916}$ valley or $\mathbf{k} = (\pm 0.85, 0)$ and $\mathbf{k} = (0, \pm 0.85)$ for the $D_{0.19}$ valleys].

$$E_{FB}^{(n)}(\mathbf{k}, k_z)A_\mu^{(n)}(\mathbf{k}, k_z) + \frac{2\pi}{L}\sum_{n',k_z'}\left\{U_T(k_z' - k_z)f_{k_z,k_z'}^{(n,n')}(\mathbf{k}, 0) + \sum_{G_z} U_T(k_z' - k_z + G_z)f_{k_z,k_z'}^{(n,n')}(\mathbf{k}, G_z)\right\} \times A_\mu^{(n')}(\mathbf{k}, k_z') = \epsilon_\mu(\mathbf{k})A_\mu^{(n)}(\mathbf{k}, k_z) \quad (1)$$

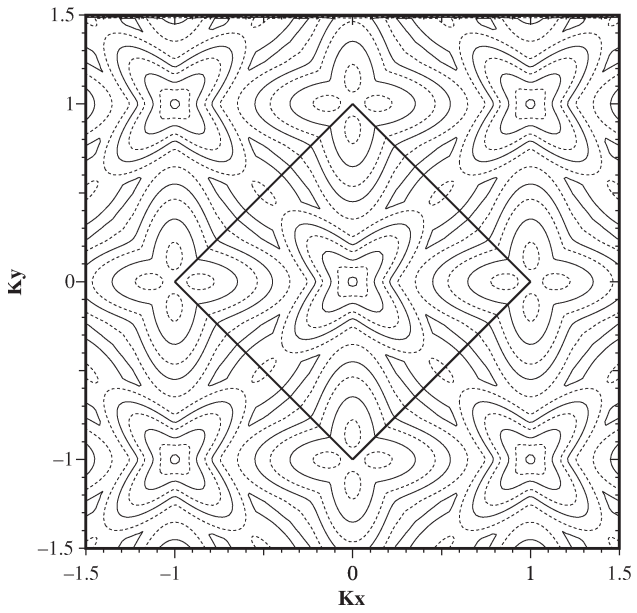

Fig. 1. Si(100). Square well with $T_{\rm SCT} = 3$ nm. Contour plot for the lowest eigenvalue $\epsilon_0(\mathbf{k})$ versus the wave vector $\mathbf{k}$ obtained by solving (1). The energy levels are 0.06, 0.4, 1.0, and 1.8 eV for the solid lines and 0.2, 0.7, 1.4, and 2.15 eV for the dashed lines. The axes are in unit of $2\pi/a_0$. The square indicates the first Brillouin zone of the 2-D electron gas. The lowest valley is the $D_{0.916}$ valley located at the point $\mathbf{k} = (0, 0)$, whereas the $D_{0.19}$ valleys are at the points $\mathbf{k} = (\pm 0.85, 0)$ and $\mathbf{k} = (0, \pm 0.85)$ (see Table I for the label of the valleys).

III. Comparison Between LCBB and EMA Results

Both the EMA and the LCBB methods can be used for any confining potential energy $U(z)$; however, we decided to compare the two models by using a very simple square well with a finite barrier U_B. The width $T_{\rm SCT}$ of the well is thus the parameter that governs the *strength* of the quantum mechanical confinement. In the following, the energy values reported in the graphs are referred to the bottom of the square well.

In the EMA approach, we assume a parabolic energy dispersion in the quantization direction with a quantization mass m_z, so that the minima of the 2-D subbands are obtained by the well-known Schrödinger-like equation in the real space [25]–[27], [38]. The eigenvalues of a square well are known in an analytical form for an infinite barrier, whereas for a finite barrier U_B, they can be obtained by solving an algebraic transcendental equation [39]. Unless it is otherwise stated (as it happens in Fig. 6), all the results shown hereafter have been obtained with a barrier $U_B = 3$ eV for both the EMA and the LCBB calculations.

The quantization mass (m_z), the transverse ($m_{\rm te}$), and the longitudinal mass ($m_{\rm le}$) employed in the EMA model are reported in Table I, and they have been obtained from the values of the longitudinal and transverse masses of the bulk crystals [40]. The effective masses for the bulk silicon and the bulk germanium (reported in the caption of Table I) have been directly extracted from the NLP calculations used as a part of the LCBB method; the values of the masses are consistent with [36] and [37].

The results of the paper are mainly focused on Si(100) transistors (which are the CMOS technology standard) and on Ge(110) devices; in fact, for the germanium n-MOSFETs, the (110) wafer orientation is the most promising among the principal orientations [12], [13], [41].

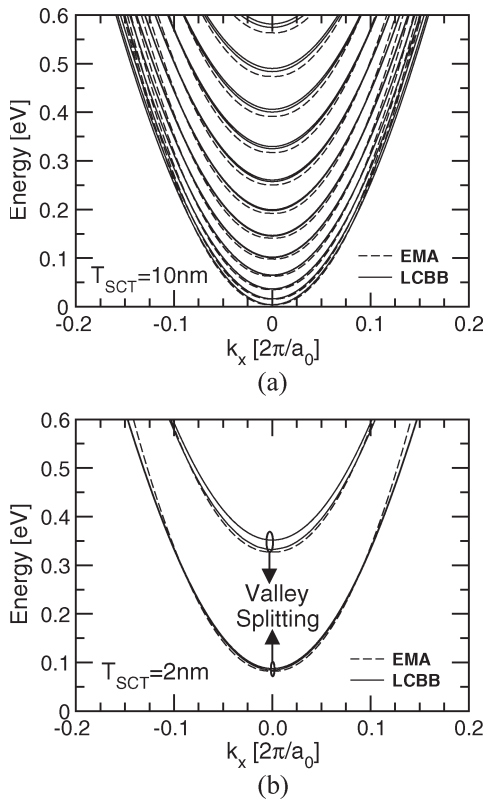

Fig. 2. Energy dispersion for the $D_{0.916}$ valley in a Si(100) inversion layer calculated with either the EMA or the LCBB model. (a) $T_{\rm SCT} = 10$ nm. (b) $T_{\rm SCT} = 2$ nm. The minimum is located at $\mathbf{k} = 0$, and k_x moves along the (010) crystal direction. Since $\mathbf{k} = 0$ is a symmetry point, exactly the same result is obtained along the (001) direction. The LCBB calculations exhibit the *valley splitting* between the doublets of subbands [25].

A. Minima of the 2-D Subbands

Fig. 2 reports the energy dispersion for Si(100) around the $D_{0.916}$ valley and for two values of $T_{\rm SCT}$. As it can be seen, the EMA approximation tracks fairly well the lowest energy branches of the LCBB band structure even for the thinnest semiconductor film. The error in the minima of the 2-D subbands increases for the higher subbands.

It is interesting to notice that the LCBB results exhibit a splitting between the two lowest subbands, which is known as valley splitting [25], and it is clearly larger in the thinner semiconductor film. The EMA model inherently assumes a perfect degeneracy for the two lowest branches of the $D_{0.916}$ valleys; hence, the valley splitting is a feature that the EMA model does not account for [25].

At this regard, Fig. 3 reports the values of the valley splitting versus the semiconductor thickness for the Si(100) $D_{0.916}$ valley. The splitting is larger for the second lowest than it is for the lowest doublet of subbands. The results for the lowest subband are in agreement with the values recently obtained with the tight-binding method [42]. The splitting for a given $T_{\rm SCT}$ is smaller than it is in a Si(100) nanowire transistor having a

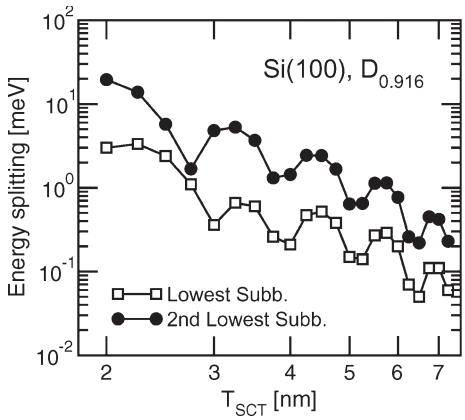

Fig. 3. Energy splitting at the minimum of the 2-D subbands versus the semiconductor thickness, calculated with the LCBB method for the Si(100) $D_{0.916}$ valleys. The results for the lowest and the second lowest doublets of subbands are illustrated. The energy splitting of the lowest subband is small compared to the thermal energy at room temperature $K_BT \simeq 26$ meV.

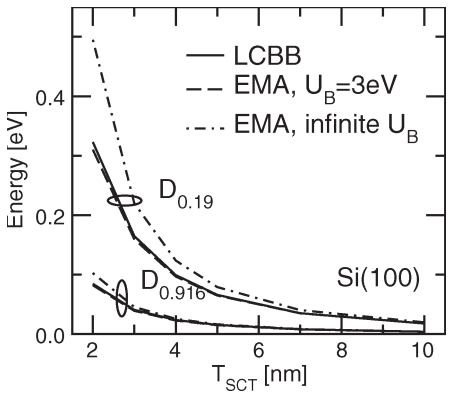

Fig. 4. Si(100). Lowest eigenvalue versus the semiconductor thickness for the $D_{0.916}$ and $D_{0.19}$ valleys that is calculated with either the LCBB or the EMA model. The EMA results for an infinite energy barrier U_B are obtained by setting the wave function to zero at the oxide interface.

diameter equal to $T_{\rm SCT}$ [30]; not surprisingly, the 2-D quantum confinement produced in a nanowire device emphasizes the valley splitting with respect to 1-D confinement in a conventional MOS transistor.

Fig. 3 shows that the *valley splitting* of the lowest subband is always small compared to the thermal energy at room temperature $K_BT \simeq 26$ meV; hence, from a practical viewpoint, it can be neglected for the analysis of the electron devices unless very low temperatures are considered.

Fig. 4 reports the minima for the lowest subband versus $T_{\rm SCT}$ for the $D_{0.916}$ and the $D_{0.19}$ valleys of Si(100). As it can be seen, the EMA approach tracks the LCBB results very well when the finite barrier $U_B = 3$ eV is accounted for. Instead, for an infinite energy barrier (which corresponds to a null boundary condition for the wave function at the semiconductor-oxide interface), the EMA minima increase well above the corresponding LCBB values for the thinnest silicon films. Fig. 5 reports the same comparison as in Fig. 4 for the $L_{0.25}$, the $D_{0.318}$, and the $\Gamma_{0.05}$ valleys of Ge(110). Even in this case, the EMA reproduces well the minima of the different valleys and their relative position, which sets the valley that gives the dominant contribution to the inversion charge and to the current of the transistor [12], [13].

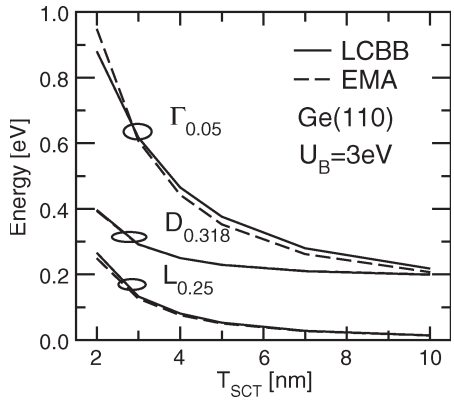

Fig. 5. Ge(110). Lowest eigenvalue versus the semiconductor thickness for the $L_{0.25}$, $D_{0.318}$, and $\Gamma_{0.05}$ valleys that is calculated with either the LCBB or the EMA model. The energy offset of the D and Γ valleys with respect to the L valleys of bulk germanium is 189 and 145 meV, respectively, as reported in Table I.

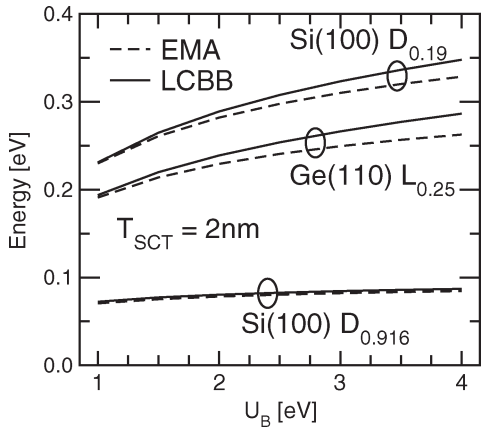

Fig. 6. Lowest eigenvalue versus the barrier height U_B for different valleys of silicon and germanium inversion layers. The semiconductor thickness is $T_{\rm SCT} = 2$ nm. As expected, the difference between the EMA and LCBB increases with U_B; the effect is more clearly observed for the small quantization masses (see Table I).

Finally, Fig. 6 illustrates the impact of the barrier height U_B on the agreement between the EMA and the LCBB calculations for some of the inversion layers considered in Figs. 4 and 5 and for the thinnest semiconductor film. As it can be seen, the differences are reduced for smaller U_B values, which are representative of some *high-k* materials actively investigated as possible SiO_2 replacements for the gate dielectric [43]. We found that, as expected, the impact of U_B on the absolute values of the subband minima and on the agreement between the EMA and LCBB calculations is significantly smaller for larger film thicknesses $T_{\rm SCT}$.

B. In-Plane Energy Dispersion and Transport Masses

In the energy dispersion illustrated in Fig. 2, we can see that the EMA can reproduce fairly well not only the subband minima but also the energy dependence on the wave vector. This implies that, in the case of Fig. 2, the values for the effective masses reported in Table I can be reliably used to describe the 2-D energy dispersion.

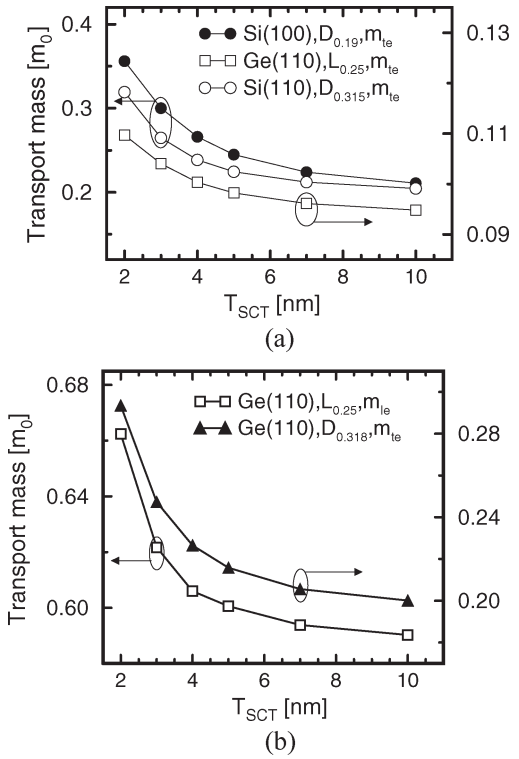

Fig. 7. Transverse ($m_{\rm te}$) and longitudinal ($m_{\rm le}$) effective masses versus the semiconductor thickness for some valleys of the Si(100) and the Ge(110) inversion layers. (a) Si(100), $\rm D_{0.19}$, $m_{\rm te}$; Ge(110), $\rm L_{0.25}$, $m_{\rm te}$; Si(110), $\rm D_{0.315}$, $m_{\rm te}$. (b) Ge(110), $\rm L_{0.25}$, $m_{\rm le}$; Ge(110), $\rm D_{0.318}$, $m_{\rm te}$. These effective masses exhibit a nonnegligible dependence on $T_{\rm SCT}$ and deviate from the values reported in Table I for very small semiconductor thicknesses.

The values of the transport masses extracted from the LCBB calculations have been systematically studied for different semiconductor thicknesses. More precisely, we have calculated the transverse $m_{\rm te}$ and the longitudinal $m_{\rm le}$ masses for the most relevant valleys of the Si(100) and the Ge(110) inversion layers by best fitting the LCBB energy dispersion. The fitting has been always performed by taking a small energy range of 10 meV above the minimum of each valley, and the transport masses have been obtained by using a strictly parabolic energy dispersion. Fig. 7 illustrates some cases where the effective masses exhibit a nonnegligible dependence on $T_{\rm SCT}$ and hence a nonnegligible deviation from the values reported in Table I and routinely employed in the EMA calculations [12], [13], [41]. The effect is particularly evident for the transverse mass in the $D_{0.19}$ valleys of Si(100).

In the cases that are not illustrated in Fig. 7, we could not identify a systematic and quantitatively relevant change of the effective masses versus $T_{\rm SCT}$. Hence, in these cases, the EMA model can be reliably used with the values for the masses of Table I (derived from the masses of the bulk crystal).

However, in addition to the possible changes of the transport masses, the LCBB calculations also reveal some differences in the 2-D band structure with respect to the EMA results that cannot be simply accounted for by adjusting the EMA parameters. In this respect, we have recently pointed out that the Si(100) inversion layers exhibit a third system of valleys (in addition to $D_{0.916}$ and $D_{0.19}$ indicated in Table I), which

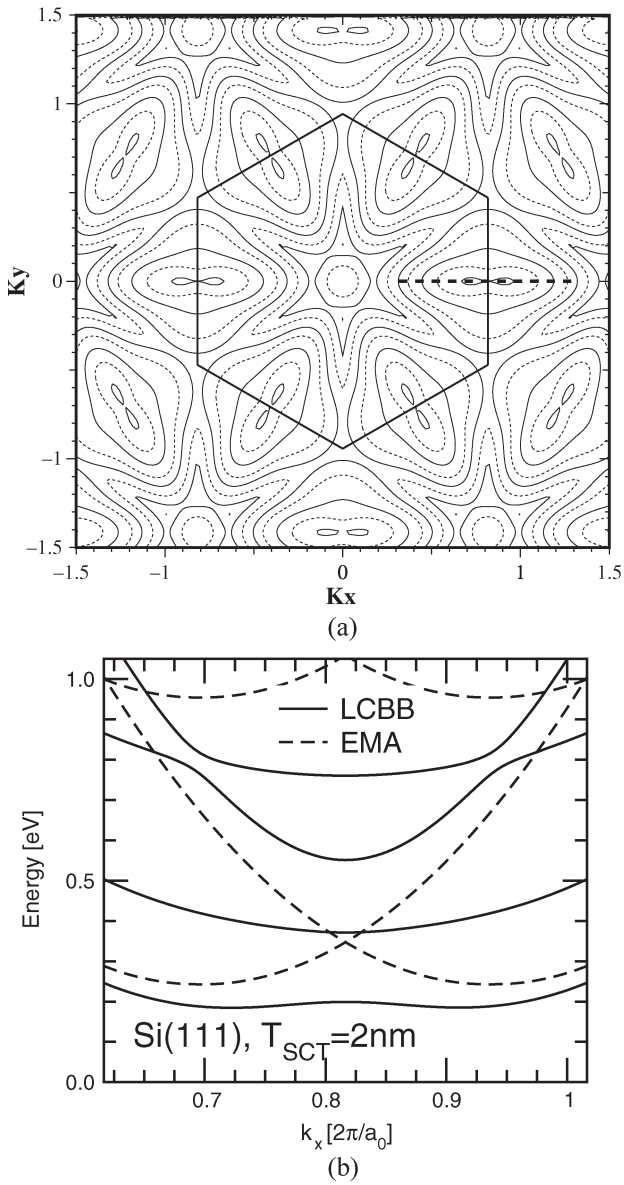

Fig. 8. Si(111). $T_{\rm SCT} = 2$ nm. (a) Contour plot for the lowest eigenvalue $\epsilon_0(\mathbf{k})$ versus the wave vector $\mathbf{k}$ that is obtained by solving (1). The energy levels are 0.2, 0.65, 1.2, and 1.8 eV for the solid lines and 0.4, 0.95, 1.5, and 2.1 eV for the dashed lines. The axes are in unit of $2\pi/a_0$. The six degenerate minima are in $\mathbf{k} = (\pm 1.7/\sqrt{6}, 0)$ and in $\mathbf{k} = (\pm 0.85/\sqrt{6}, \pm 0.85/\sqrt{2})$. The hexagon indicates the 2-D Brillouin zone [34]. (b) Energy dispersion along the dashed line indicated in (a) obtained with either the LCBB or the EMA model. The minimum of the LCBB calculations is no longer at the point $k_x = 1.7/\sqrt{6}$, as for thicker silicon films. Furthermore, the minimum predicted by the EMA overestimates the corresponding LCBB value.

is located at the boundary of the 2-D Brillouin zone, and it is typically neglected in the EMA picture [34], [35].

A case of a similarly large discrepancy between the EMA and LCBB results is illustrated in Fig. 8 for the Si(111) inversion layer. In fact, Fig. 8(a) shows the energy dispersion of the lowest subband in the $\mathbf{k}$ plane and for $T_{\rm SCT} = 2$ nm. The hexagon indicates the 2-D Brillouin zone, and the minimum along the positive k_x direction is at $k_x = 1.7/\sqrt{6} \simeq 0.694$, as expected from the position of the energy minima in the 3-D Brillouin zone [34], [40]. However, Fig. 8(b) shows that for $T_{\rm SCT} = 2$ nm, the minimum calculated by the LCBB method

tends to move toward the edge of the 2-D Brillouin zone (i.e., at $k_x = 2.0/\sqrt{6} \simeq 0.8165$), and its value is significantly overestimated by the EMA model. Furthermore, the LCBB band structure exhibits a flat energy branch that corresponds to an effective mass much larger than the $m_{\rm le} = 0.674$ value reported in Table I (and that is anyway difficult to be reproduced with a simple parabolic or nonparabolic model).

C. Density of States

In order to further compare the LCBB and the EMA models, we have studied the 2-D electron density of states (DOS), which is a very important parameter because it is tightly related to the calculation of the scattering rates. The EMA model has analytical expressions for the 2-D DOS for both the parabolic and nonparabolic cases [26], [27], [38]. For the LCBB model, instead, the DOS has been numerically calculated by counting for each energy bin the $\mathbf{k}$ points in the 2-D first Brillouin zone that have an eigenvalue belonging to the energy bin. Each $\mathbf{k}$ point must be weighted for an appropriate area in the $\mathbf{k}$ plane according to the $\mathbf{k}$ discretization, which leads to the following mathematical expression

$$D_{\rm 2D}(E) = \sum_{\mu,k_x,k_y} \frac{2\Delta k_x \Delta k_y}{(2\pi)^2 \Delta E} \left\{ H\left[\epsilon_\mu(k_x,k_y) - E + \frac{\Delta E}{2}\right] - H\left[\epsilon_\mu(k_x,k_y) - E - \frac{\Delta E}{2}\right] \right\} \quad (2)$$

where ΔE, Δk_x, and Δk_y indicate the spacing in the energy and in the $\mathbf{k}$ discretization, whereas $H(x)$ is the step function.

Fig. 9 compares the EMA to the LCBB DOS curves for Si(100) and for $T_{\rm SCT} = 3$ and 2 nm. The EMA results have been obtained either for the transport masses of Table I or for the values corrected according to the $T_{\rm SCT}$ dependence shown in Fig. 7. As it can be seen, the conventional two-valley picture typically employed in the EMA approach tends to underestimate the DOS. By including the contribution of the X-valley at the edge of the 2-D Brillouin zone [34], [35] and by employing the $T_{\rm SCT}$-dependent transport masses, the agreement between the EMA and the LCBB results becomes good up to energies around 0.6 eV above the lowest minimum. This is the energy range of practical interest to simulate the $I_{\rm DS}$ in the transistors of modern CMOS technologies, where the supply voltage is 1 V or below.

Fig. 10 shows the comparison between the EMA and the LCBB DOS for Ge(110). Even in this case, the agreement is fairly good in the range of most practical interest, and the use of the $T_{\rm SCT}$ dependent masses reported in Fig. 7 makes the EMA results closer to the LCBB calculations. For Si(111), instead, Fig. 11 shows that the agreement between the EMA and the LCBB results is worse. In particular, in the case of $T_{\rm SCT} = 2$ nm, the LCBB DOS features a peak at an energy

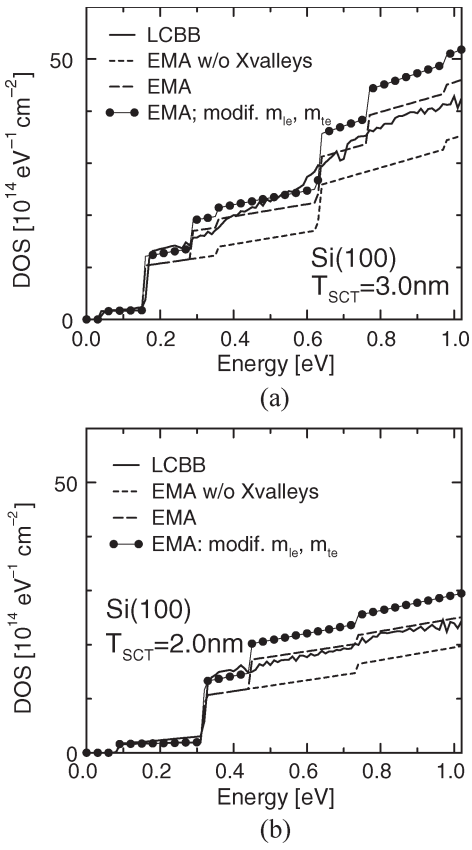

Fig. 9. Electron 2-D DOS versus energy for Si(100) that is obtained with either the LCBB or the EMA model. (a) $T_{\rm SCT} = 3$ nm. (b) $T_{\rm SCT} = 2$ nm. The EMA nonparabolic model that employs only the $D_{0.916}$ and $D_{0.19}$ valleys tends to underestimate the DOS calculated by the LCBB method. A better agreement with the LCBB calculations is obtained by adding the X-valley to the EMA model [34]. For the EMA case, we show (dashed and long-dashed lines) the results that employ the transport masses defined in Table I and (filled circles) the results that have been obtained by using for each $T_{\rm SCT}$ value the corresponding transport masses reported in Fig. 7. In this latter case, the X-valleys have been accounted for.

appreciably lower than the lowest available states according to the EMA model. This peak of DOS clearly stems from the flat energy branch in the LCBB energy dispersion illustrated in Fig. 8(b), which results in a DOS that decreases with the energy for very low energy values. This latter behavior cannot be reproduced by an EMA model, even if we adjust the masses. Hence, we conclude that, in the case of Si(111) and at very small silicon thicknesses, it is problematic to follow the LCBB results with an EMA approach.

IV. Discussion and Conclusion

In this paper, we have systematically investigated the validity of the EMA quantization model for the silicon and the germanium n-MOSFETs with different crystal orientations. To this purpose, we have used the LCBB full-band quantization model to study the main parameters that govern the electron density and the transport in the inversion layers: the minima of the 2-D subbands, the transport masses, and the 2-D DOS.

The comparison of the EMA results to the LCBB calculations indicates that the simplified EMA approach can quite

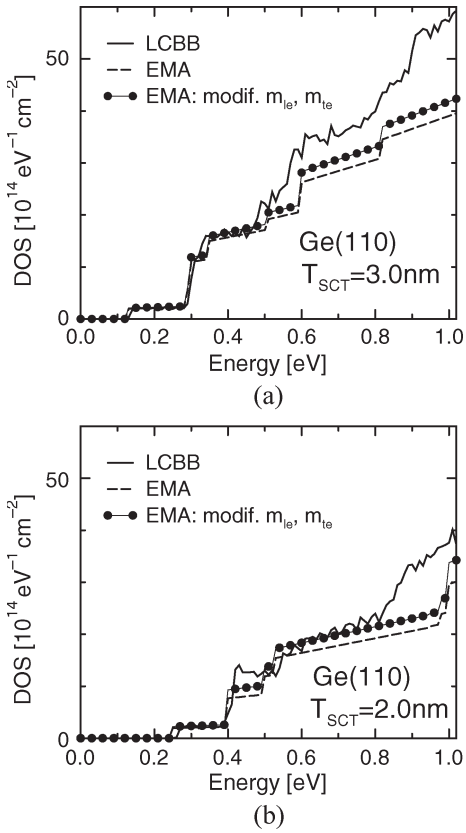

Fig. 10. Electron 2-D DOS versus energy for Ge(110) that is obtained with either the LCBB or the EMA model. For the EMA case, we show the results that employ the transport masses defined in Table I and the results that have been obtained by using for each $T_{\rm SCT}$ value the corresponding transport masses reported in Fig. 7. (a) $T_{\rm SCT} = 3$ nm. (b) $T_{\rm SCT} = 2$ nm. The agreement of the EMA to the LCBB calculations is fairly good up to an energy about 0.6 eV above the minimum of the lowest subband.

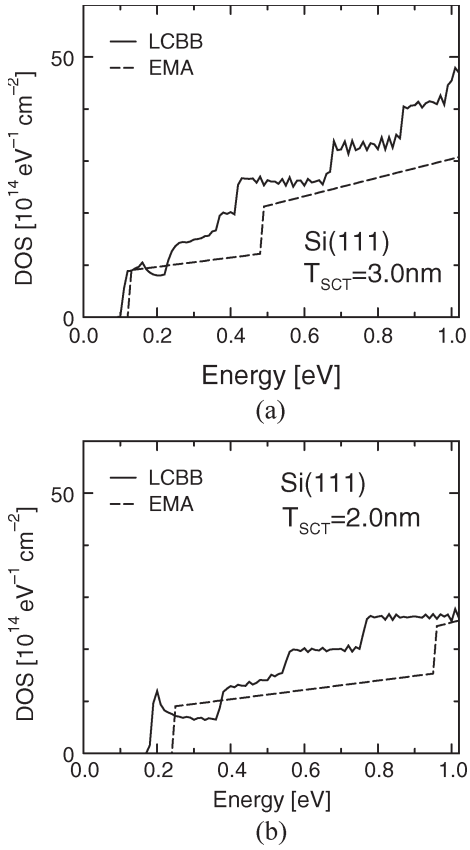

Fig. 11. Electron 2-D DOS versus energy for Si(111) that is obtained with either the LCBB or the EMA model. (a) $T_{\rm SCT} = 3$ nm. (b) $T_{\rm SCT} = 2$ nm. In the case of the thinnest semiconductor film, we see a clear peak of the DOS according to the LCBB calculations at energies below the lowest states obtained with the EMA model.

accurately reproduce the minima of the 2-D subbands provided that a finite value of the semiconductor–oxide barrier is accounted for. When the EMA is used with a null boundary condition for the wave function at the semiconductor–oxide interface, instead, the results for $T_{\rm SCT}$ values below approximately 5 nm significantly deviate from the LCBB calculations, which inherently employ a finite semiconductor–oxide barrier.

In some quantization directions, the LCBB method points out that by scaling $T_{\rm SCT}$, the 2-D energy dispersion is not merely shifted (as it happens in an EMA model), but an appreciable distortion of the energy to $\mathbf{k}$ relation is produced. We have quantified this effect by extracting from the LCBB calculations the effective transport masses and illustrated their possible dependence on $T_{\rm SCT}$ and the deviations from the values typically employed in the EMA model.

In most cases, the changes of the transport masses are modest, at least for the crystal directions of largest technological interest. However, in some cases, the LCBB approach points out that the confining potential energy changes the position of the energy minima in the 2-D Brillouin zone and produces branches in the 2-D energy dispersion that are hard to be reproduced with a simple parabolic or nonparabolic model [see the discussion of Figs. 8 and 11 for the Si(111) inversion layers].

As a general conclusion, it can be stated that the EMA model is fairly reliable even for very thin silicon films; in some cases, its accuracy can be improved by changing the transport masses as illustrated in Fig. 7. Our results have been obtained by using a schematic, square well, confining potential. However, we verified that the main trends are fully verified even in a triangular well; hence, they are expected to be of general validity for the electron inversion layers of n-MOS transistors.

ACKNOWLEDGMENT

The authors would like to thank Prof. J. Schmitz for his constant support and encouragement during this work.

REFERENCES

[1] M. Jurczak, T. Skotnicki, M. Paoli, B. Tormen, J. Martins, J. L. Regolini, D. Dutartre, P. Ribot, D. Lenoble, R. Pantel, and S. Monfray, "Silicon-on-nothing (SON)—An innovative process for advanced CMOS," *IEEE Trans. Electron Devices*, vol. 47, no. 11, pp. 2179–2187, Nov. 2000.

[2] E. Suzuki, K. Ishii, S. Kanemaru, T. Maeda, T. Tsutsumi, T. Sekigawa, K. Nagai, and H. Hiroshima, "Highly suppressed short-channel effects in ultrathin SOI n-MOSFETs," *IEEE Trans. Electron Devices*, vol. 47, no. 2, pp. 354–359, Feb. 2000.

[3] D. Esseni, M. Mastrapasqua, G. K. Celler, C. Fiegna, L. Selmi, and E. Sangiorgi, "Low field electron and hole mobility of SOI transistors fabricated on ultra-thin silicon films for deep sub-micron technology application," *IEEE Trans. Electron Devices*, vol. 48, no. 12, pp. 2842–2850, Dec. 2001.

[4] D. Esseni, M. Mastrapasqua, G. K. Celler, C. Fiegna, L. Selmi, and E. Sangiorgi, "An experimental study of mobility enhancement in ultra-thin SOI transistors operated in double-gate mode," *IEEE Trans. Electron Devices*, vol. 50, no. 3, pp. 802–808, Mar. 2003.

[5] K. Uchida, J. Koga, R. Ohba, and T. S. Takagi, "Experimental evidences of quantum–mechanical effects on low-field mobility, gate-channel capacitance and threshold voltage of ultrathin body SOI MOSFETs," in *IEDM Tech. Dig.*, 2001, pp. 633–636.
[6] K. Uchida, H. Watanabe, A. Kinoshita, J. Koga, T. Numata, and S. Takagi, "Experimental study on carrier transport mechanisms in ultrathin-body SOI n- and p-MOSFETs with SOI thickness less than 5 nm," in *IEDM Tech. Dig.*, 2002, pp. 47–50.
[7] K. Morimoto, T. Hirai, K. Yuki, and K. Morita, "Fabrication and transport properties of silicon quantum wire gate-all-around transistor," *Jpn. J. Appl. Phys.*, vol. 35, no. 2B, pp. 853–857, 1996.
[8] Y. S. Tang, G. Lin, J. H. Davies, J. G. Williamson, and C. D. W. Wilkinson, "Quantized conductance in a long silicon inversion wire," *Phys. Rev. B, Condens. Matter*, vol. 45, no. 23, pp. 13 799–13 802, 1992.
[9] M. Je, S. Han, I. Kim, and H. Shin, "A silicon quantum wire transistor with one-dimensional subband effects," *Solid State Electron.*, vol. 44, no. 12, pp. 2207–2212, Dec. 2000.
[10] J. Wang, E. Polizzi, and M. Lundstrom, "A computational study of ballistic silicon nanowire transistors," in *IEDM Tech. Dig.*, 2003, pp. 695–698.
[11] C. M. Lieber, "Nanowires as building blocks for nanoelectronics and nanophotonics," in *IEDM Tech. Dig.*, 2003, pp. 300–302.
[12] T. Low, Y. T. Hou, M. F. Li, C. Zhu, A. Chin, G. Samudra, L. Chan, and D. L. Kwong, "Investigation of performance limits of germanium double-gated MOSFETs," in *IEDM Tech. Dig.*, 2003, p. 691.
[13] S. E. Laux, "Simulation study of Ge n-channel 7.5 nm DGFETs of arbitrary crystallographic alignment," in *IEDM Tech. Dig.*, 2004, p. 135.
[14] A. Pethe, T. Krishnamohan, D. Kim, S. Oh, H. S. P. Wong, Y. Nishi, and K. C. Saraswat, "Investigation of the performance limits of III–V double-gate n-MOSFETs," in *IEDM Tech. Dig.*, 2005, pp. 605–608.
[15] A. Rahman, G. Klimeck, and M. Lundstrom, "Novel channel materials for ballistic nanoscale MOSFETs: Bandstructure effects," in *IEDM Tech. Dig.*, 2005, pp. 601–604.
[16] J. Welser, J. L. Hoyt, S. Takagi, and F. Gibbons, "Strain dependence of the performance enhancement in strained-Si n-MOSFETs," in *IEDM Tech. Dig.*, 1994, pp. 373–376.
[17] K. Rim, J. L. Hoyt, and F. Gibbons, "Fabrication and analysis of deep submicron strained-Si n-MOSFETs," *IEEE Trans. Electron Devices*, vol. 47, no. 7, pp. 1406–1415, Jul. 2000.
[18] T. Mizuno, N. Sugiyama, T. Tezuka, T. Numata, and S. Takagi, "High-performance strained-SOI CMOS devices using thin film SiGe-on-insulator technology," *IEEE Trans. Electron Devices*, vol. 50, no. 4, pp. 988–994, Apr. 2003.
[19] T. Mizuno, N. Sugiyama, T. Tezuka, Y. Moriyama, S. Nakaharai, and S. Takagi, "[110]-surface strained-SOI CMOS devices," *IEEE Trans. Electron Devices*, vol. 52, no. 3, pp. 367–374, Mar. 2005.
[20] M. Lundstrom, "Elementary scattering theory of the Si MOSFET," *IEEE Electron Device Lett.*, vol. 18, no. 7, pp. 361–363, Jul. 1997.
[21] F. Assad, Z. Ren, D. Vasileska, S. Datta, and M. Lundstrom, "On the performance limits for Si MOSFET's: A theoretical study," *IEEE Trans. Electron Devices*, vol. 47, no. 1, pp. 232–240, Jan. 2000.
[22] P. Palestri, D. Esseni, S. Eminente, C. Fiegna, E. Sangiorgi, and L. Selmi, "Understanding quasi-ballistic transport in nano-MOSFETs. Part I: Scattering in the channel and in the drain," *IEEE Trans. Electron Devices*, vol. 52, no. 12, pp. 2727–2735, Dec. 2005.
[23] S. Eminente, D. Esseni, P. Palestri, C. Fiegna, L. Selmi, and E. Sangiorgi, "Understanding quasi-ballistic transport in nano-MOSFETs. Part II: Technology scaling along the ITRS roadmap," *IEEE Trans. Electron Devices*, vol. 52, no. 12, pp. 2736–2743, Dec. 2005.
[24] L. Lucci, P. Palestri, D. Esseni, and L. Selmi, "Multi-subband Monte Carlo modeling of nano-MOSFETs with strong vertical quantization and electron gas degeneration," in *IEDM Tech. Dig.*, 2005, pp. 631–634.
[25] T. Ando, A. Fowler, and F. Stern, "Electronic properties of two-dimensional systems," *Rev. Mod. Phys.*, vol. 54, no. 2, pp. 437–672, Apr. 1982.
[26] M. V. Fischetti and S. E. Laux, "Monte Carlo study of electron transport in silicon inversion layers," *Phys. Rev. B, Condens. Matter*, vol. 48, no. 4, pp. 2244–2274, Jul. 1993.
[27] C. Jungemann, A. Edmunds, and W. L. Engl, "Simulation of linear and nonlinear electron transport in homogeneous silicon inversion layers," *Solid State Electron.*, vol. 36, no. 11, pp. 1529–1540, 1993.
[28] S. C. Williams, K. W. Kim, and W. C. Holton, "Ensemble Monte Carlo study of channel quantization in a 25 nm n-MOSFET," *IEEE Trans. Electron Devices*, vol. 47, no. 10, pp. 1864–1872, Oct. 2000.
[29] S. E. Laux, A. Kumar, and M. V. Fischetti, "Analysis of quantum ballistic electron transport in ultrasmall silicon devices including space-charge and geometric effects," *J. Appl. Phys.*, vol. 95, no. 10, pp. 5545–5582, 2004.
[30] J. Wang, A. Rahman, A. Ghosh, G. Klimeck, and M. Lundstrom, "On the validity of the parabolic effective-mass approximation for the I–V calculation of silicon nanowire transistors," *IEEE Trans. Electron Devices*, vol. 52, no. 7, pp. 1589–1595, Jul. 2005.
[31] J. L. van der Steen, D. Esseni, P. Palestri, and L. Selmi, "Validity of the effective mass approximation in silicon and germanium inversion layers," in *Proc. Int. Workshop Comput. Electron.*, 2006, p. 301.
[32] L. Wang and A. Zunger, "Linear combination of bulk bands method for large-scale electronic structure calculations on strained nanostructures," *Phys. Rev. B, Condens. Matter*, vol. 59, no. 24, pp. 15 806–15 818, 1999.
[33] F. Chirico, A. Di Carlo, and P. Lugli, "Efficient Self-consistent pseudopotential calculation of nanostructured devices," *Phys. Rev. B, Condens. Matter*, vol. 64, no. 4, p. 045 314, Jun. 2001.
[34] D. Esseni and P. Palestri, "Linear combination of bulk bands method for investigating the low-dimensional electron gas in nanostructured devices," *Phys. Rev. B, Condens. Matter*, vol. 72, no. 16, pp. 165 342.1–165 342.14, 2005.
[35] D. Esseni and P. Palestri, "Fullband quantization analysis reveals a third valley in (001) silicon inversion layers," *IEEE Electron Device Lett.*, vol. 26, no. 6, pp. 413–415, Jun. 2005.
[36] J. R. Chelikowsky and M. L. Cohen, "Nonlocal pseudopotential calculations for the electronic structure of eleven diamond and zinc-blende semiconductors," *Phys. Rev. B, Condens. Matter*, vol. 14, no. 2, pp. 556–582, 1976.
[37] M. V. Fischetti and J. M. Higman, "Theory and calculation of the deformation potential electron-phonon scattering rates in semiconductors," in *Monte Carlo Device Simulation: Full Band and Beyond*. K. Hess, Ed., Norwell, MA: Kluwer, 1991, ch. 5.
[38] D. K. Ferry and S. M. Goodnick, *Transport in Nanostructures*. Cambridge, U.K.: Cambridge Univ. Press, 1997.
[39] D. K. Ferry, *Quantum Mechanics—An Introduction for Device Physicists and Electrical Engineers*. Bristol, U.K.: Inst. Phys. Publishing, 1995.
[40] F. Stern and W. E. Howard, "Properties of semiconductor surface inversion layers in the electric quantum limit," *Phys. Rev.*, vol. 163, no. 3, pp. 816–835, 1967.
[41] M. De Michielis, D. Esseni, and F. Driussi, "Trade-off between electron velocity and density of states in ballistic nano-MOSFETs," in *Proc. Eur. Solid State Device Res. Conf.*, 2005, pp. 165–168.
[42] T. B. Boykin, G. Klimeck, M. Friesen, S. N. Coppersmith, P. von Allmen, F. Oyafuso, and S. Lee, "Valley splitting in low-density quantum-confined heterostructures studied using tight-binding models," *Phys. Rev. B, Condens. Matter*, vol. 70, no. 16, p. 165 325, Oct. 2004.
[43] G. D. Wilk, R. M. Wallace, and J. M. Anthony, "High-k gate dielectrics: Current status and materials properties considerations," *J. Appl. Phys.*, vol. 89, no. 10, pp. 5243–5275, 2001.

Jan-Laurens P. J. van der Steen (S'06) was born in Wageningen, The Netherlands, on December 26, 1980. He received the M.Sc. degree in electrical engineering from the University of Twente, Enschede, The Netherlands, in 2006. He is currently working toward the Ph.D. degree in the Semiconductor Components Group, MESA+ Institute for Nanotechnology, University of Twente.

His research topic is device physics, with a focus on modeling and simulation of carrier transport in very thin semiconductor layers.

David Esseni (S'98–M'00–SM'06) received the Laurea and Ph.D. degrees in electronic engineering from the University of Bologna, Bologna, Italy, in 1994 and 1998, respectively.

In 1999, he became an Assistant Professor and, later on, an Associate Professor at the University of Udine, Udine, Italy. In 2000, he was a Visiting Scientist at Bell Laboratories, Lucent Technologies, Murray Hill, NJ. His research activities include the characterization techniques for electrical parameters in MOS devices and several aspects related to the hot-electron phenomena in MOSFETs and Flash EEPROMs. In particular, he has studied the reliability of thin-oxide transistors, the statistical distribution of stress-induced leakage current in Non Volatile Memory (NVM) arrays, and the low-voltage and substrate-enhanced hot-electron injection for applications to Flash EEPROM devices. More recently, he was been involved in the experimental characterization and in the modeling of low-field mobility in ultrathin silicon-on-insulator MOSFETs and in MOSFETs with ultrathin gate oxides. His modeling interests also include the quantization in MOS devices beyond the effective mass approximation and the semiclassical Monte Carlo approach for deca–nanometric MOSFETs.

Dr. Esseni has served as a member of the technical committee of the International Electron Devices Meeting in 2003–2004. He is currently in the technical committee of the European Solid State Device Research Conference and of the International Reliability Physics Symposium. He is a member of the Technology Computer Aided Design Committee of the Electron Device Society (EDS).

Pierpaolo Palestri (M'05) received the Laurea degree (*summa cum laude*) in electronic engineering from the University of Bologna, Bologna, Italy, in 1998, and the Ph.D. degree in electronic engineering from the University of Udine, Udine, Italy, in 2003.

In 1998, he was with the Department of Electrical, Mechanical, and Management Engineering, University of Udine, as a Research Assistant in the field of device simulation. From July 2000 to September 2001, he held a postdoctoral position at Bell Laboratories–Lucent Technologies (now Agere Systems), Murray Hill, NJ, where he worked on high-speed silicon–germanium bipolar technologies. In October 2001, he became an Assistant Professor at the University of Udine and became an Associate Professor in November 2005. His research interests include the modeling of carrier transport in nanoscale devices and the simulation of hot-carrier and tunneling phenomena in scaled MOSFETs and nonvolatile memory cells.

Luca Selmi (M'01) was born in 1961. He received the Ph.D. degree in Electrical Engineering from the University of Bologna, Bologna, Italy, in 1992.

From 1989 to 1990, he was a Visiting Scientist at Hewlett Packard Microwave Technology Division, Santa Rosa, CA. In 2000, he became a Full Professor of Electronics at the University of Udine, Udine, Italy. Since 2001, he has been holding the same position in the "Circuit and Interconnect Reliability" subcommittee. His research interests include characterization and simulation of silicon devices, with emphasis on Monte Carlo transport techniques and hot-carrier effects in MOSFETs and nonvolatile memory cells, leakage currents, reliability of ultrathin oxides, and device optimization. These activities have been conducted in cooperation with international research centers such as Bell Laboratories, IBM T. J. Watson Research Center, Philips Research Laboratories, Institut National Polytechnique de Grenoble and LETI Grenoble. He coauthored approximately 120 papers, including 26 International Electron Devices Meeting (IEDM) papers.

Dr. Selmi was a member of the IEDM technical subcommittee on "Modeling and Simulation" from 1995 to 1996.

Raymond J. E. Hueting (S'94–M'98–SM'06) was born in Bussum, The Netherlands, on May 28, 1968. He received the M.Sc. (*cum laude*) and Ph.D. degrees in electrical engineering from the Delft University of Technology, Delft, The Netherlands, in 1992 and 1997, respectively. For both degrees, the subject was device modeling and characterization of high-speed SiGe-based heterojunction devices.

In 1997, he joined Philips Semiconductors, Nijmegen, The Netherlands, where he worked on SOI-based BCD-IC processes. In 1998, he joined Philips Research Laboratories, Eindhoven, The Netherlands. In 2001, he joined Philips Research, Leuven, Belgium, where he was involved with the development of novel silicon devices, among which are SiGe-based heterojunction devices and trench power MOSFETs. In 2004, he joined the laboratory of Semiconductor Components, University of Twente, Enschede, The Netherlands, where he is involved with device modeling. He authored and coauthored more than 15 papers and 60 patents, 23 of which are U.S. patents.

Dr. Hueting participated in the technical program committee of the International Symposium on Power Semiconductor Devices & ICs (ISPSD) Conference, Japan, in 2004.